



Enhanced sustained release of furosemide in long circulating chitosan-conjugated PLGA nanoparticles

Sapna Kashyap^{1,*}, Amit Singh¹, Abha Mishra², and Vikas Singh^{3,*}

¹Department of Pharmacology, Institute of Medical Sciences, Banaras Hindu University, Varanasi -221005, India.

²School of Biochemical Engineering, Indian Institute of Technology, Banaras Hindu University, Varanasi -221005, India.

³Department of Chemical Engineering, Indian Institute of Technology-Delhi, New Delhi- 110016, India.

Abstract

Furosemide (FSM) is commonly used in the treatment of edema associated with congestive cardiac failure, cirrhosis of the liver, renal disease, including the nephrotic syndrome and hypertension. However, in ascites, it is clinically limited due to its frequent dosing and short biological half-life and its prolonged-release preparations are not available. Therefore, the main objective behind the present research work is to develop chitosan coated and conjugated poly (lactic-co-glycolic acid) (PLGA) nanocarriers, to sustain the delivery of FSM with improved systemic circulation. Emulsion-solvent evaporation technique was used for the preparation of nanoparticles. *In-vivo* pharmacokinetic study showed 2.6, 3.10, and 4.30 folds enhancement in relative availability of FSM for FSM-PLGA, FSM-chitosan-coated-PLGA and FSM-chitosan-conjugated-PLGA nanoparticles, respectively than FSM. The present research work concluded that FSM loaded chitosan conjugated PLGA nanoparticles could enhance the systemic circulation of FSM with improved pharmacokinetics parameters.

Keywords: Chitosan; FSM; Nanocarriers; PLGA; Polymeric nanoparticles; Sustained effect.

INTRODUCTION

Furosemide (FSM), is a loop diuretic (1) being used in the treatment of edematous states associated with cardiac, renal and hepatic failure and in treatment of hypertension (2). It inhibits the $\text{Na}^+/\text{K}^+/\text{2Cl}^-$ transporter in the ascending limb of the loop of Henle (3). FSM is available in the oral and intravenous (i.v.) formulations and i.v. FSM is twice as potent as oral FSM (4). The diuretic effect of oral FSM is apparent within 30 min to 1 h and is maximal in the first or second hour. The duration of action is usually 6-8 h. After i.v. administration of FSM, diuresis occurs within 5 min, reaches a maximum within 20-60 min, and persists for approximately 2 h. FSM is approximately 95% bound to plasma proteins in healthy individual (2). However, in patients with severe liver cirrhosis and ascites, hypoalbuminemia occurs and i.v. FSM is recommended to be administered frequently that may lead to patient non-compliance (5).

Since no prolong release preparations of FSM is available (2), we have tried to formulate long circulating chitosan coated and conjugated poly (lactide-co-glycolide) (PLGA) nanocarriers to sustain the delivery of FSM. Further, it has been reported that co-polymeric nanocarriers are emerging as safe and alternate delivery system and have achieved significant success in overcoming the challenges of delivery and residence time and have been extensively studied to develop nanocarriers drug delivery system (NCDDS) (6). PLGA, an FDA approved non-cytotoxic, biocompatible and biodegradable polymer, is being investigated as NCDDS for sustained drug delivery (7,8). PLGA is a product obtained due to co-polymerization of poly lactic acid (PLA) and poly glycolic acid (PGA) which exhibits decent mechanical properties, low immunogenicity, low toxicity, and a predictable pharmacokinetic property (9).

Corresponding authors:
S. Kashyap, Tel: +91-9580382082; Fax: +91-5422367568
Email: sapna7399@gmail.com
V. Singh, Tel: +91-9540316547; Fax: +91-1126581120
Email: ch1150143@iitd.ac

Access this article online



Website: <http://rps.mui.ac.ir>

DOI: 10.4103/1735-5362.253356

Because of presence of methyl side groups in side chains of PLA, it is less hydrophilic than PGA and hence lactide rich PLGA co-polymer are more hydrophobic, absorbs less water and subsequently degrade more slowly (10).

PLGA can be synthesized in size range of 10-1000 nm and can be used to encapsulate FSM (11). When the diameter of carrier is less than the diameter of the smallest blood capillaries (4 μ m), parenteral administration of drug loaded NCDDS can be facilitated, curtailing any possible embolism (12). The degradation of PLGA occurs through hydrolysis of ester linkages. The biodegradation of PLGA changes its properties which affects the release and degradation rate of encapsulated drug molecules (10).

Additionally, literature reviews suggest that the dose and composition of NCDDS affect blood clearance and uptake by the mononuclear phagocyte system (13). Moreover, the whole body autoradiography and quantitative distribution experiments indicate that PLGA nanoparticles accumulate rapidly in the liver, bone marrow, lymph nodes, spleen, and peritoneal microphagous (14). The PLGA exhibits a non-linear and dose-dependent biodistribution and pharmacokinetics and it degrades rapidly at the initial stage (approximately 30%) and slows subsequently (15).

The impact of surface modification have been studied in order to minimize above challenges and incorporation of hydrophilic polymers such as chitosan as surface modifying agent can significantly improve its systemic circulation and half-life (sustain release property) (16). Chitosan, a derivative of chitin, is a biodegradable, biocompatible cationic polymer (17) with low toxicity, remarkably increases cellular uptake of PLGA NCDDS (18). Further, modifying the PLGA surfaces with chitosan also reduces the opsonization by phagocytic mononuclear systems and hence is less susceptible to reticuloendothelial system (RES) uptake and decreased accumulation resulted in liver and spleen (19).

Hence, prolonged release action of FSM loaded chitosan-conjugated PLGA

nanoparticles could be achieved. It has been evidenced that chitosan modified PLGA nanocarriers prevents the entrapped drug from oxidation hence retaining the antioxidant activity of the bioactive ingredients to deliver it effectively to the cells without causing any possible adverse effects to the cells (20). Additionally, in the presence of chitosan, colloidal behavior of PLGA nanoparticles have also been studied and it was observed that the surface charge of the particle was reduced because of strong electrical interactions (21) and thus improving stability of resulting NCDDS (22). It has been reported that the positively charged PLGA-chitosan nanoparticles get attracted by negatively charged cellular membranes resulting in enhanced cellular uptake (16).

Based on the above mentioned facts, it has been anticipated that the surface modification of PLGA particles by hydrophilic polymer chitosan could limit the opsonisation and hence restricts RES (monocytes, macrophages, and kupffer cells) recognition, ensuring prolong systemic circulation of FSM. The reduced uptake by RES and enhanced residence time of FSM in blood circulation could open up new avenues to overcome frequent dosing and non-patient compliance in patients suffering with severe liver cirrhosis.

MATERIALS AND METHODS

Materials

PLGA with a L/G ratio of 75:25, MW 66-107 kDa and inherent viscosity of 0.55-0.75 dL/g and Tween 80 were purchased from Sigma Aldrich (Sigma Aldrich, Saint-Louis, MO, USA). FSM of purity 99%, chitosan (extra-pure), 2-(N-morpholino) ethanesulfonic acid (MES), 4-(2-hydroxyethyl)-1-piperazineethanesulfonic acid (HEPES), acetic acid, sodium hydroxide and sodium carbonate were purchased from Sisco Research Laboratories, (Mumbai, India). 1-(3-Dimethyl aminopropyl)-3-3-ethylcarbodiimide hydrochloride (EDC), N-hydroxy succinimide (NHS), and ethyl acetate were purchased from Himedia Laboratories, (Mumbai, India). Methanol was purchased from Loba Chemie Pvt. Ltd, (New Delhi, India).

Methods

Statistical model

A 2³ full factorial model has been used for optimization of diuretic drug loaded nanocarriers. The three independent variables taken are amount of FSM, a diuretic drug as X₁, amount PLGA as X₂, amount of chitosan as X₃. The parameters that were studied as a function of these independent variables are particle size (Y₁), polydispersity index (Y₂), and percentage of encapsulation (Y₃). It is assumed that all the parameters depend on all the three independent variables X₁-X₃. It is further assumed that the result also depend on interaction between these variables that are X₁X₂, X₁X₃, X₂X₃. The following equation was used.

$$Y = b_0 + b_1X_1 + b_2X_2 + b_3X_3 + b_4X_1X_2 + b_5X_1X_3 + b_6X_2X_3.$$

In the above equation, X_i for i = 1, 2, 3 are the independent variable, Y is the dependent variable and b_i, for i = 1, 2, 3 are measure of the change in average Y for change in corresponding X_i from low to high value. The analysis was done using JMP 13 trial version.

Formulation of FSM-loaded PLGA nanoparticles

Conventional methodology of O/W emulsion-solvent was used for formulation of FSM-loaded PLGA nanoparticles. Drug (6 mg) was added to PLGA (13 mg) ethyl acetate (3 mL) polymeric solution and emulsified in 7 mL of 1 % Tween 80 aqueous solution. The resultant emulsion was subjected for further stirring at a speed of 12,000 rpm for 20 min at 4 °C by using Remi C-24 cold centrifuge to obtain the nanoparticles and was subsequently washed twice, with MES buffer (100 mM) in double distilled water. Then, the double washed nanoparticles were redispersed by using Spinix-vortex shaker (23).

Preparation of chitosan-coated PLGA nanoparticles

Chitosan coating onto the PLGA nanoparticles was achieved by adding 3 mL chitosan solution (0.2% (w/v)) in aqueous acetic acid (1% (w/v)) to the PLGA nanoparticle suspension in MES buffer (24).

Preparation of chitosan-conjugated PLGA nanoparticles

Activation of carboxylic groups of PLGA was achieved by NHS and EDC (0.1 M solution) by dissolving 0.115 g of NHS and 0.19 g of EDC in 10 mL of HEPES buffer (20 mM). NHS (5 mL) and EDC (0.1 M solution) was added to PLGA nanoparticle suspension, followed by 3 h stirring at room temperature and 20 min centrifugation at 10,000 rpm at 4 °C. The obtained nanoparticles were washed in distilled water (5 mL) and re-suspended in HEPES buffer (5 mL) followed by sonication using a Spinix-vortex. Chitosan-conjugated PLGA nanoparticles were obtained by addition of chitosan suspension (5 mL) to the activated PLGA nanoparticle suspension followed by 12 h stirring at room temperature and 20 min centrifugation at 10,000 rpm at 4 °C (25).

Nanoparticles characterization

Drug polymer compatibility by FTIR spectroscopy

FTIR spectra's of chitosan, PLGA, FSM, chitosan-conjugated PLGA, blank and FSM loaded nanoparticles were obtained by using KBr pellet method using FTIR spectrophotometer (Perkin Elmer Spectrum Two, Waltham, Massachusetts, USA).

Particle size and surface charge analysis

Photon correlation spectroscopy was used to determine the particle size of PLGA nanoparticles, chitosan-coated PLGA, and chitosan-conjugated PLGA nanoparticles using Zetasizer (Malvern instruments Ltd, Malvern, UK).

Zeta potential

The surface electric charge of nanoparticles, depicted as zeta potential was measured by Zetasizer ver. 7.03 (Malvern instruments Ltd, Malvern, UK).

Surface morphology

Scanning electron microscope

Surface morphology of PLGA, chitosan-coated PLGA, and chitosan-conjugated PLGA nanoparticles were visualized using EVO-18, MA15/18 (ZEISS Supra 40) and scanning

electron microscope (SEM) images were obtained at 30 KX magnifications and at electron beam voltage (EHT) of 5 kV.

Transmission electron microscope study

Surface morphology of PLGA and chitosan modified nanoparticles were performed using Tecnai G2 20 TWIN analytical transmission electron microscope (TEM). 10 µg/mL nanoparticles were dried on copper grids and images captured after staining.

Atomic force microscopy study

The NTEGRA PRIMA-atomic force microscope (AFM) NT-MDT was used in tapping mode, at high resonant frequency and scan speed of 0.5 Hz. The measurements were obtained using AFM image analysis software (NOVA-Px-3.1.0-Rev 3880).

Powder X-ray diffraction study

Miniflex 300/600 automated desktop X-ray diffraction system (Rigaku) was used for powder X-ray diffraction (PXRD) analysis using Ni-filtered Cu K α radiation at 40 kV and 15 mA. Angle of diffraction was analyzed from 5° to 50° with step width of 0.05° and scan speed of 4°/min. PDXL software (Rigaku) was used for interpretation of diffraction patterns (26). Since, the tape was used during XRD for PLGA sample, the diffraction pattern of blank tape (graph 4G) was also taken into account to eliminate its XRD characteristic peaks while analyzing XRD data of PLGA.

In vitro drug release studies

FSM release pattern from PLGA nanoparticles, chitosan-coated PLGA, and chitosan-conjugated PLGA nanoparticles was studied using dialysis membrane diffusion method. Specifically, 1 mL of nanoparticle suspension was taken into inner dialysis membrane (molecular weight cut off 12-14 kDa, Himedia laboratories, Mumbai, India), hermetically sealed and immersed into 20 mL of 0.1% (v/v) of Tween 80 aqueous solution of alkaline phosphate buffer (pH 7.4) followed by stirring at 100 rpm at 37 °C. From the outer media, samples (1 mL) were withdrawn at predetermined time intervals of

2, 4, 6, 8, 10, 12 h and the sink condition was maintained by replacing the withdrawn amount with freshly prepared phosphate buffer. The FSM content was determined by UV spectrophotometer (Shimadzu 1800, Tokyo, Japan) at 276 nm and the percent drug release was calculated at each time point interval (27).

In vivo pharmacokinetic study

Animal handling and caring protocols, approved by the Institute of Medical Sciences (IMS), Banaras Hindu University (BHU), were followed. Charles foster adult male rats (200-250 g) were provided by Central Animal House (IMS, BHU) and taken care at departmental animal room of pharmacology (IMS, BHU). One week prior to the experiments, the animals were acclimatized to normal room temperature and relative humidity of 50-60% under natural light/dark conditions and given appropriate feed and water. The study guidelines of Committee for the Purpose of Control and Supervision on Experiments on Animals were approved (Registration No. Dean/2018/CAEC/817). After acclimatization for one week, 4 animal groups (3 treatment groups including PLGA, chitosan-coated PLGA, and chitosan-conjugated PLGA; and one control group) with 3 rats in each group, were recruited. Control group (group 1) received an i.v. injection of suspension of the FSM (6.6 mg/kg of FSM), group 2 received an i.v. injection of PLGA nanoparticle (6.6 mg/kg of FSM), group 3 received an i.v. injection of chitosan-coated-PLGA nanoparticle (6.6 mg/kg of FSM) and group 4, received an i.v. injection of chitosan-conjugated-PLGA nanoparticle (6.6 mg/kg of FSM). Dosage requirement was met by concentrating the nanoparticles to 1 mL. For groups 2-4, blood samples were collected at time interval of 0, 2, 4, 6, 8, 12, and 24 h after administration of nanoformulations and for group 1, blood samples were collected at time interval of 0, 2, 4, 6, 8 h after administration of FSM suspension. Plasma samples for HPLC analysis were prepared by 10 min centrifugation at 11,000 rpm and stored at -20 °C (28).

To the 50 μL of serum, 5 μL of p-nitrophenol (1100 $\mu\text{g}/\text{mL}$, internal standard) was added. The samples were acidified with 5 μL of 2 M H_3PO_4 , followed by extraction with ethyl acetate (200 μL), dried under N_2 (gas) and restored in 30 μL of mobile phase [0.01 M KH_2PO_4 (pH 5.5)- MeOH (63:37, v/v)]. Subsequently, 20 μL sample was injected to the column. HPLC system comprised of a Shimadzu LC-20 AD HPLC pump and a model SPD-M20A 230 V Shimadzu UV-visible detector and a Nucleosil C18 (250 \times 4.6 mm I.D., particle size 10 nm) analytical column. The detector operates at 276 nm and the flow rate was isocratic at 1.5 mL min^{-1} . Retention time for this system for FSM and p-nitrophenol were 8.275 and 10.059 min, respectively.

The FSM concentration in plasma was determined using the standard curve obtained for known concentrations of FSM in plasma (29).

Statistical analysis

Results are being represented as mean \pm standard deviation (SD). Student's t-test was used for comparison of mean data of particle diameter, encapsulation efficiency,

in vitro and *in vivo* results. Results corresponding to the value of $P < 0.05$ were considered as significant.

RESULTS

The effect of independent variables (X_1, X_2, X_3) on the dependent variables (Y_1, Y_2, Y_3) using the 2^3 full factorial model, led to the Pareto plot (Fig. 1A) and the cube plot (Fig. 1B) to draw the inference. In the cube plot, which was plotted for Y_1 , the independent variable X_1 when moved along the edge of the cube for which X_2 and X_3 were constant, changing it from the lower to higher values; significant variation was observed in the value of Y_1 . Similarly, when X_2 was moved from lower to higher value along the respective edges, changes in the corresponding values of Y_1 , was quite low as compared to case with X_1 , but result is significant for both the variables. It was further observed that the corresponding changes in the values of Y_1 with change in X_3 from low to high value along the three edges of the cube is in accordance with the variation observed in X_2 and X_3 but along one edge it showed deviation.

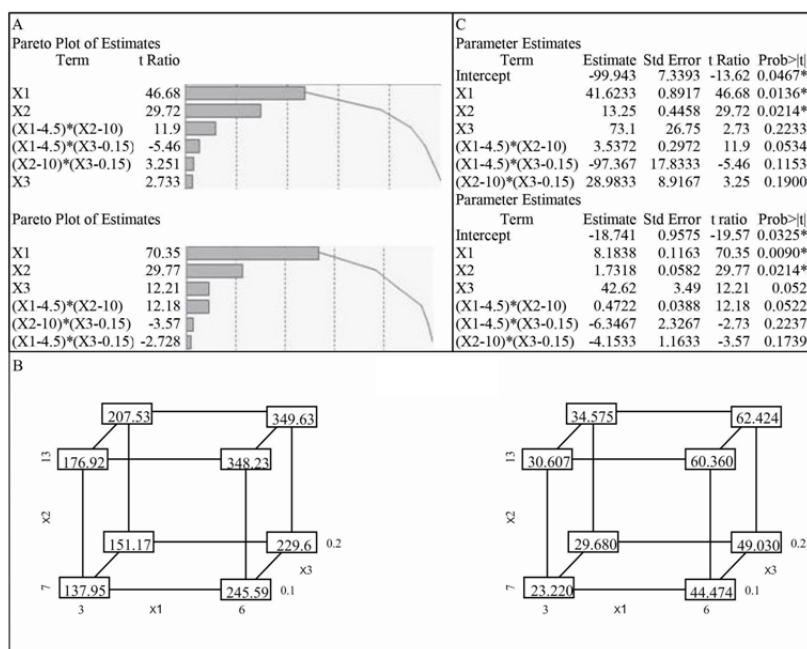


Fig. 1. (A) Pareto plot showing the effect of the formulation variable and their interaction on the size (top) and on the percentage encapsulation (bottom), (B) cube plot for the mean particle size (on left) and for the percentage encapsulation (on right) with the formulation variables, (C) parameter estimate showing the P value for the mean particle size (top) and for the percentage encapsulation (bottom).

Table 1. Dependent and independent variables for various formulations prepared in this research work.

Batches	X ₁ (mg)	X ₂ (mg)	X ₃ (%)	Y ₁ (nm)	Y ₂	Y ₃ (%)
F1	6	13	0.2	350.9675	0.920	62.25
F2	6	7	0.1	246.9275	0.705	44.30
F3	6	13	0.1	346.8925	0.915	60.53
F4	3	7	0.1	136.6125	0.450	23.39
F5	3	13	0.1	178.2575	0.460	30.43
F6	3	7	0.2	152.5075	0.503	29.50
F7	6	7	0.2	228.2625	0.880	49.20
F8	3	13	0.2	206.1925	0.530	34.75

X₁, Furosemide; X₂, poly (lactide-co-glycolide); X₃, chitosan; Y₁, particle size; Y₂, polydispersity index; Y₃, encapsulation efficiency.

Similar inference can be drawn from the Pareto plot and parameter estimate (Fig. 1C), the value of *P* obtained are *P* = 0.0136 for X₁, *P* = 0.0214 for X₂, and *P* = 0.2233 for X₃. The significantly low value of X₁ shows its dominant contribution. While the relatively high value of *P* for X₂ shows its less dominance yet significant contribution in Y₃, but the value of *P* for X₃ is > 0.05 hence the contribution of X₃ in determining the Y₁ is insignificant though high value of X₃ is required which can be explained as, moving from low value (0.1) to high value (0.2) along the three edges of the cube in the cube plot resulted increased particle size and along one edge it resulted decrease in particle size which may be due the negative interaction (X₁X₃) value of -5.46 (Fig. 1C). The interaction term that is X₁X₂, X₁X₃, and X₂X₃ all have their *P* value > 0.05 so are insignificant and hence have negligible contribution to the Y₁. The R² = 0.99 which shows that our model can explain 99% of the deviations in the value of Y₁.

Similarly, for the Y₃ and the independent variables X₁, X₂, and X₃ from Fig. 1C, we obtain the similar result that is the dominant effect of X₁ with *P* value of 0.0090 and less dominant yet significant for X₂ with *P* value of 0.0214, and the insignificant contribution of X₃ with *P* value of 0.0520. But the high value of X₃ is explained by the cube plot. The interaction term X₁X₂, X₁X₃, X₂X₃ have *P* value greater than 0.05 and hence are not affecting Y₃. The R² value of 0.99 for this case also shows that our model can explain 99% of the deviations in the value of Y₃. The model does not fit on Y₂ as the overall *P* value comes out to be greater than > 0.05. The best result is

obtained for higher value of X₁, higher value X₂ and higher value of X₃ for all the three cases. From the Pareto plot it was evident that the FSM amount (X₁) has a significant effect on particle size (Y₁) with the *P* value of 0.0136 (*P* < 0.05) (Fig. 1C) which can be clearly figured out from Table 1 i.e. with the increase in the X₁ (6 mg) in batches F1, F2, F3, and F7, the particle size increases and with the decrease in the X₁ (3 mg) in batches F4, F5, F6, and F8 particle size decreases. A similar inference can be drawn for PLGA amount (X₂) with *P* value of 0.0214 (*P* < 0.05) (Fig. 1C). The least effect of chitosan amount (X₃) with *P* value of 0.2233 (*P* > 0.05) (Fig. 1C) is justified because of the low molecular weight of chitosan.

FTIR spectroscopy analysis

Band at 3400.11 cm⁻¹ in chitosan spectrum (Fig. 2A), indicates the combined peaks of the -NH₂ and -OH group stretching. A distinctive absorption bands appear at 1662.70 cm⁻¹ (amide I), 1605.37 cm⁻¹ (-NH₂ bending), and 1393.88 cm⁻¹ (amide III). The absorption bands at 1142 cm⁻¹ (asymmetric stretching of the -COOOC- bridge), 1072 cm⁻¹, and 1052 cm⁻¹ (skeletal vibration involving the -COO stretching) are characteristic of its saccharine structure. Characteristic peak of PLGA has been reported at 1752.07 cm⁻¹ because of ester group (Fig. 2B) (30). Chitosan conjugation to PLGA was established by amide bond formation, observed at weak band of 1643.49 cm⁻¹ (amide I band) and a strong band of 1574.31 cm⁻¹ (amide II band) (Fig. 2C). In chitosan-coated nanoparticles these two amide bands were absent (Fig. 2D).

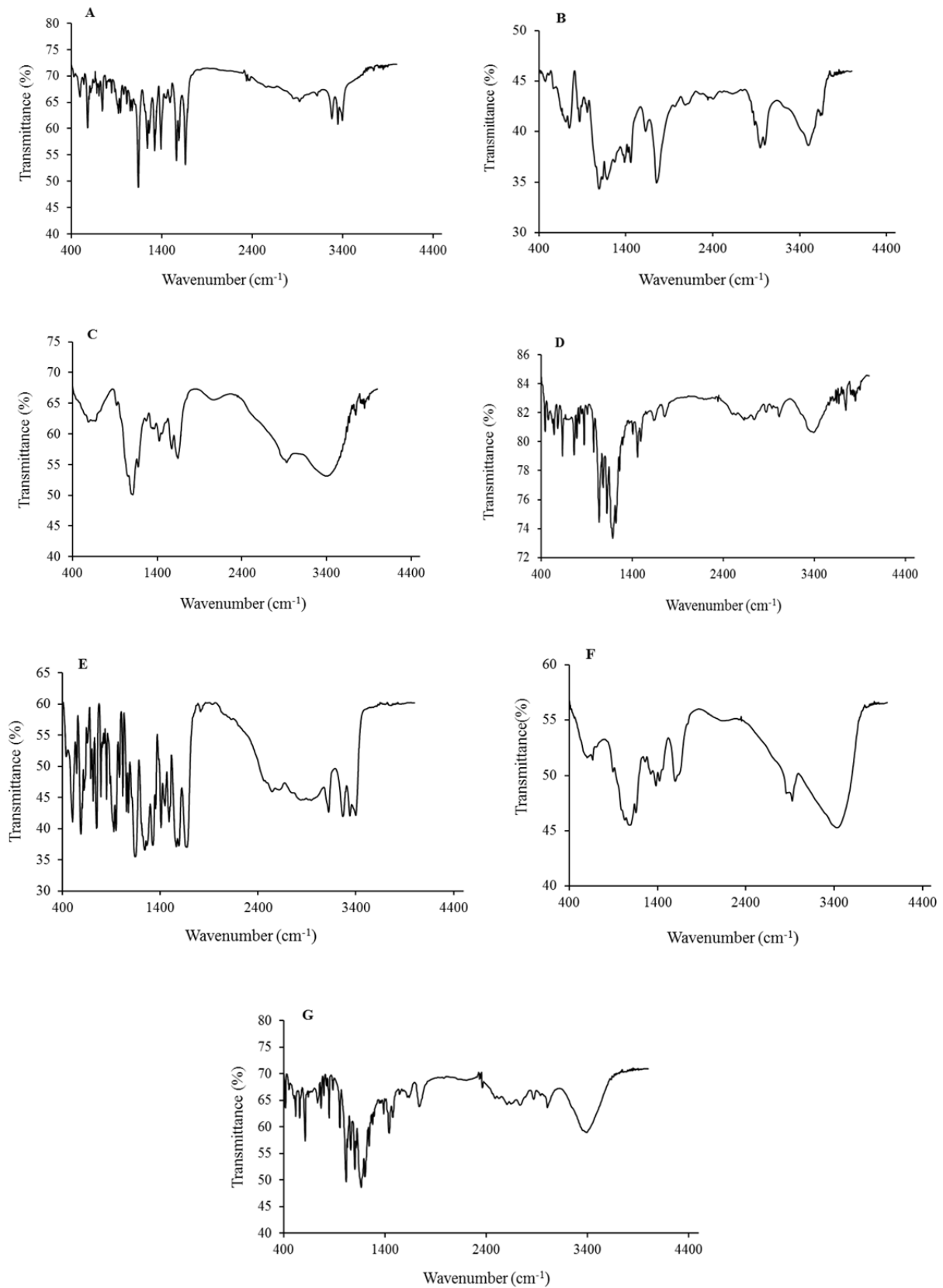


Fig. 2. Fourier-transform infrared spectroscopy spectra of (A) chitosan, (B) PLGA, (C) chitosan-conjugated PLGA nanoparticles, (D) chitosan-coated PLGA nanoparticles, (E) FSM, (F) blank nanoparticles, (G) FSM-loaded nanoparticles. PLGA, poly (lactide-co-glycolide); FSM, furosemide.

The characteristic peak representing saccharine structure of chitosan is present in both chitosan-coated and chitosan-conjugated PLGA nanoparticles.

Characteristic peak of FSM was seen at 3400 cm^{-1} , 3260 cm^{-1} , 1665 cm^{-1} , and 1560 cm^{-1} (26). The 3400 cm^{-1} band shows stretching vibration of $-\text{NH}_2$ in aromatic ring while the 3260 cm^{-1} band shows stretching vibration of $-\text{SO}_2\text{NH}_2$, and 1665 cm^{-1} band shows bending vibration of the $-\text{NH}_2$. The band 1560 cm^{-1} is characterized by carbonyl group asymmetric stretching vibration. The sulfonyl group presents in FSM is characterized by its asymmetric stretching vibration at 1318 cm^{-1} band (26). From FSM spectra, sharp characteristic peaks at 3401.61 cm^{-1} , 3123.56 cm^{-1} , 1665.28 cm^{-1} , and 1565.13 cm^{-1} were shown in spectra (Fig. 2E). The characteristic peaks of PLGA and chitosan are present in the blank nanoparticles spectra (Fig. 2F). Spectra of FSM-loaded nanoparticles shows characteristic peaks of FSM, PLGA, and chitosan without showing any significant shift in the absorption peaks (Fig. 2G).

Zeta potential and particle size

The zeta potential (mV) of PLGA nanoparticles was found to be negative ($-20.0 \pm 2.36\text{ mV}$) which could be due to the presence of terminal carboxyl groups (26). The zeta potential of the chitosan nanoparticles (chitosan-coated and chitosan-conjugated nanoparticles) was found to be less negative which could be due to the presence of terminal amine group (19). The mean diameters of the PLGA nanoparticles were $282.22 \pm 1.53\text{ nm}$, chitosan-coated PLGA nanoparticles were $319.88 \pm 1.90\text{ nm}$, and chitosan-conjugated-PLGA nanoparticles were $352.08 \pm 1.70\text{ nm}$

(Table 2). Thus, the diameters of nanoparticles have been observed in the range of 200 to 500 nm (Fig. 3C₃). As evident, the incorporation of chitosan to PLGA nanoparticles resulted in increment in particle diameter which was explained by the cube plot (Fig. 1B).

Surface morphology analysis

Scanning electron microscopy

The SEM images of the PLGA, chitosan-coated, and chitosan-conjugated nanoparticles are shown in Fig. 3A₁-3C₁ in $1\text{ }\mu\text{m}$ scale, that shows the particle size $< 500\text{ nm}$. SEM images exhibit smooth surfaced and spherical shaped particles.

Transmission electron microscopy

Figure 3A₂-3C₂ depicts TEM images of PLGA, chitosan-coated, and chitosan-conjugated nanoparticles. The surface topography indicates a smooth surface without any perforations and cracks and was almost uniform in size. Spherical shape of chitosan-coated and chitosan-conjugated nanoparticles in its peripheral shell as well was confirmed by TEM images. The particles sizes are also in agreement with the results obtained from photon correlation spectroscopy (PCS) and SEM.

Atomic force microscopy analysis

The 2 dimensional (2D) and 3D AFM images are shown in Fig. 3A₃ and Fig. 3B₃ respectively. The morphological studies performed by AFM showed uniform and spherical shaped discrete particles without aggregation and smooth in surface morphology with a nano size range of 200 to 400 nm which agrees well with PCS, SEM, and TEM.

Table 2. Particle size and zeta potential of poly (lactide-co-glycolide) (PLGA) and chitosan modified PLGA nanoparticles; (n = 3).

Formulation	Particle size (nm) (mean \pm SD)	Zeta potential (mV) (mean \pm SD)	Drug loading (%) (mean \pm SD)	Encapsulation (%) (mean \pm SD)
PLGA nanoparticles	282.22 ± 1.53	-20.0 ± 2.36	20.24 ± 3.2	64.10 ± 4.7
Chitosan-coated PLGA nanoparticles	319.88 ± 1.90	-11.7 ± 1.27	22.03 ± 2.4	69.79 ± 4.2
Chitosan-conjugated PLGA nanoparticles	352.08 ± 1.70	-9.1 ± 1.31	20.26 ± 1.3	64.18 ± 3.9

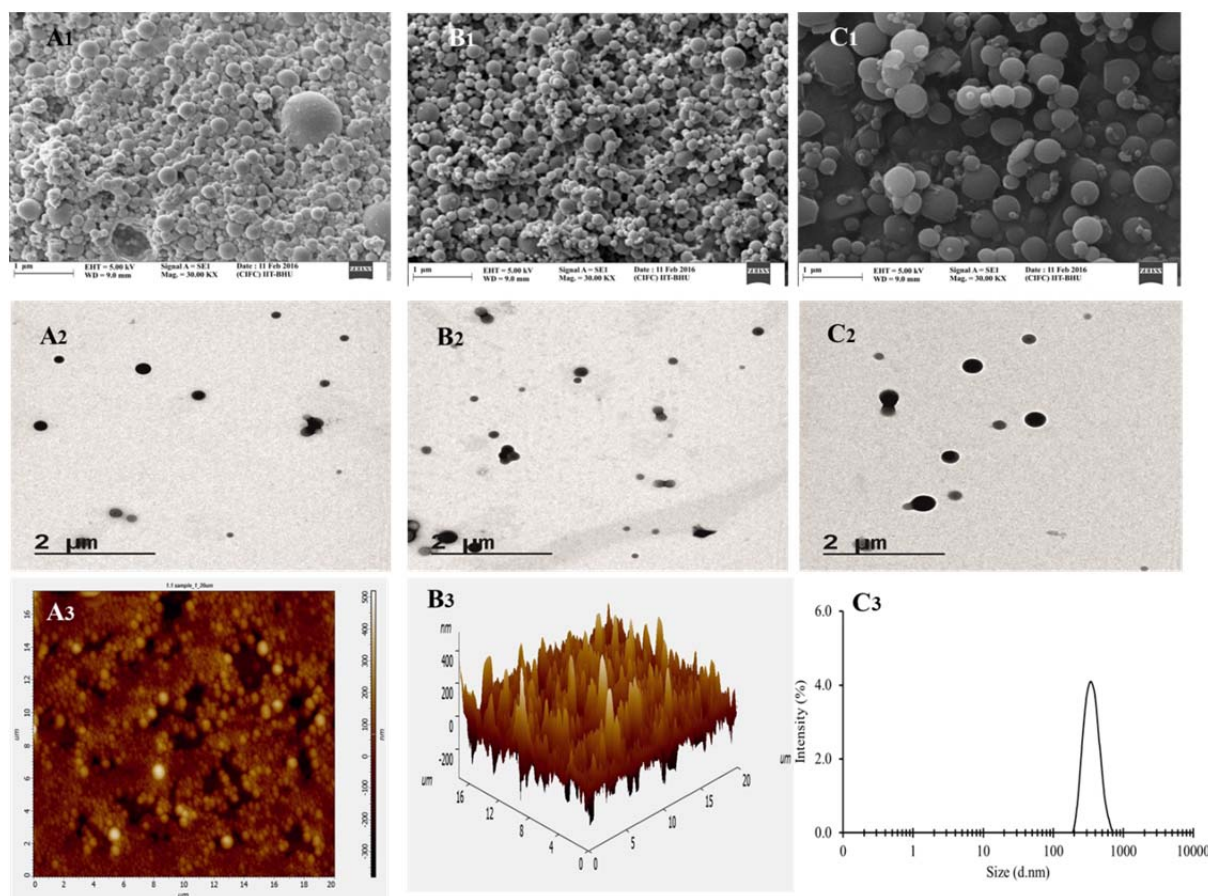


Fig. 3. Scanning electron microscope (SEM) image of (A₁) PLGA nanoparticles, (B₁) FSM loaded chitosan-coated PLGA nanoparticles, (C₁) FSM loaded chitosan-conjugated PLGA nanoparticles; transmission electron microscope (TEM) image of (A₂) PLGA nanoparticles, (B₂) FSM loaded chitosan-coated PLGA nanoparticles, (C₂) FSM loaded chitosan-conjugated PLGA nanoparticles; (A₃ and B₃) atomic force microscope (AFM) 2D and 3D images of fFSM loaded chitosan-conjugated PLGA nanoparticles respectively, (C₃) particle size distribution of FSM loaded chitosan-conjugated PLGA nanoparticles depicted by Zetasizer. PLGA, poly (lactide-co-glycolide); FSM, furosemide.

Powder X-ray diffraction analysis

The PXRD patterns of the native FSM, chitosan, PLGA, blank nanoparticles, and FSM physical mixture (1:1, w/w), FSM-loaded chitosan coated, conjugated PLGA nanoparticles, and tape are shown in Fig. 4A-G respectively. As previously reported⁽²⁶⁾, the major peaks of FSM were found to be at a diffraction angle of 11.8°, 18°, 18.5°, 22.1°, 23.9°, and 28.0° respectively (Fig. 4A). Since 75% lactic acid in PLGA imparts amorphous behavior of the polymer, no crystalline peaks were seen in XRD of PLGA (Fig. 4C). Chitosan amorphous nature was confirmed by absence of any diffraction peak (Fig. 4B). Diffraction patterns of physical mixture of FSM and blank nanoparticles (Fig. 4D) showed almost similar peak intensity as in XRD of FSM. FSM-loaded chitosan coated (Fig. 4E) and conjugated PLGA

nanoparticles (Fig. 4F) showed decreased peak intensities at the same diffraction angle of FSM suggesting reduced degree of crystallinity of FSM. Comparing the diffraction patterns of physical mixture of FSM and blank nanoparticles (Fig. 4D) and FSM-loaded nanoparticles (Fig. 4E), no significant crystalline deviation was observed, indicating the presence of FSM in the crystal state.

Determination of encapsulation efficiency

Drug encapsulation efficiency of the PLGA, chitosan-coated, and chitosan-conjugated nanoparticles was found to be $64.10 \pm 4.7\%$, $69.79 \pm 4.2\%$, and $64.18 \pm 3.9\%$ respectively (Table 2). Enhanced drug encapsulation efficiency of the chitosan coated nanoparticles in comparison to PLGA nanoparticles could be due to the addition of chitosan at the

surface of the PLGA nanoparticles and conjugated nanoparticles shows almost similar encapsulation efficiency to the PLGA nanoparticles is probably due to the drug loss during the formulation process that may get

adhere to the surface of the beaker. The percentage drug loading of the PLGA nanoparticles and conjugated nanoparticles were found to be $20.24 \pm 3.2 \mu\text{g}/\text{mg}$ and $22.03 \pm 2.4 \mu\text{g}/\text{mg}$ respectively (Table 2).

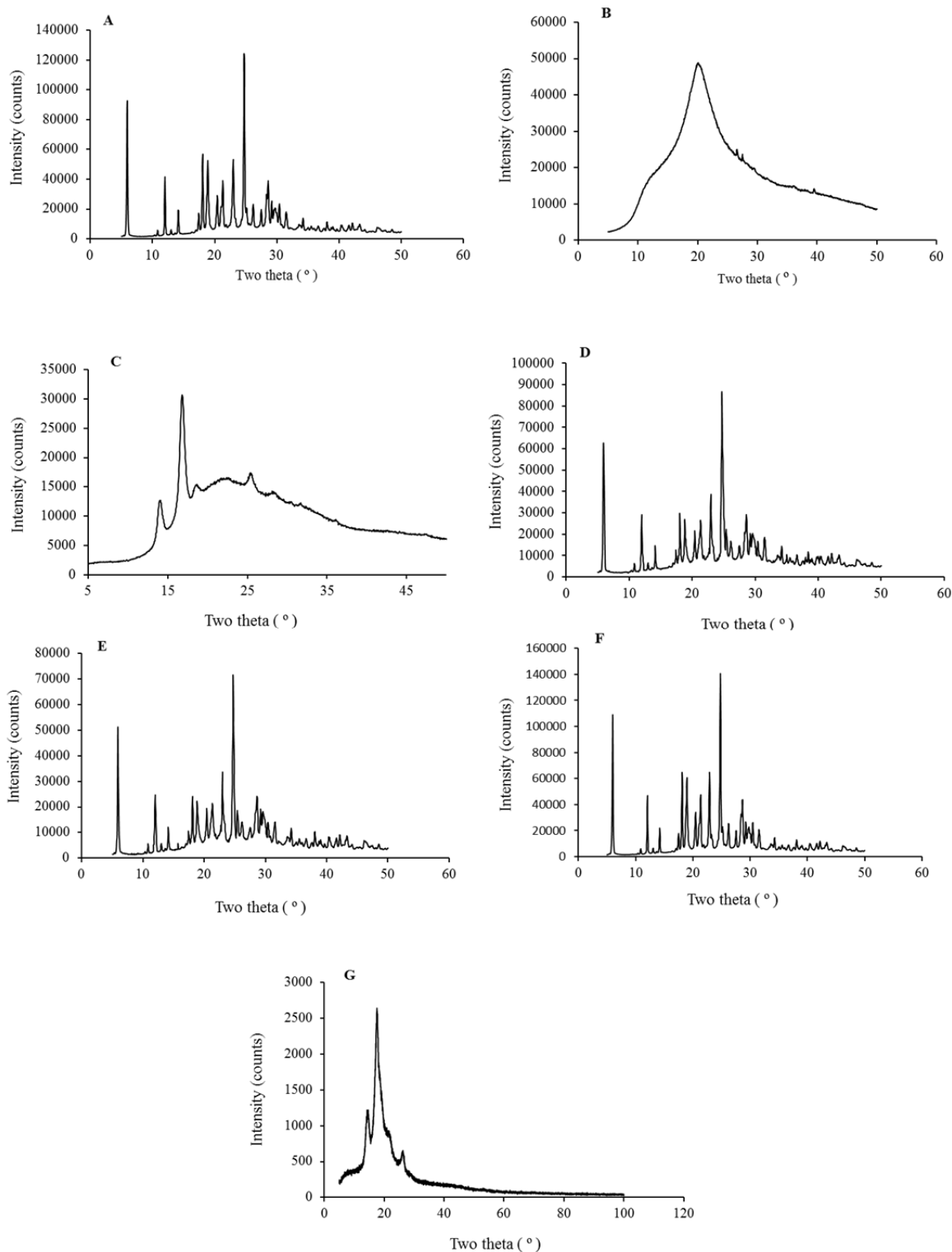


Fig. 4. Powder X-ray diffraction pattern for (A) FSM (pure), (B) chitosan, (C) PLGA, (D) FSM loaded chitosan-coated PLGA nanoparticles, (E) FSM loaded chitosan-conjugated PLGA nanoparticles, (F) blank nanoparticles and FSM (physical mixture, 1:1, w/w), and (G) tape used in XRD of PLGA. PLGA, Poly (lactide-co-glycolide); FSM, furosemide.

In vitro drug release studies

Chitosan modified PLGA nanoparticles showed an *in vitro* drug release of 55.76% and 50.65% (Fig. 5A) from chitosan-coated and chitosan-conjugated PLGA nanoparticles respectively in 6 h, which agrees well with the result obtained by pharmacokinetic study. These nanoparticles showed a sustained release pattern for 12 h. After 12 h of *in vitro* drug release studies the FSM released from the formulations was 86.45%, 74.72%, and 70.23% respectively for the PLGA, chitosan-coated, and chitosan-conjugated nanoparticles.

In vivo pharmacokinetic study

Fig. 5B depicts the FSM concentration in the plasma vs time curve obtained after an i.v. injection of FSM suspension, FSM loaded PLGA nanoparticles and FSM-chitosan-conjugated PLGA nanoparticles to Charles foster rats at FSM concentration of 6.6 mg/kg (n = 3). Phoenix Winolin 6.4 software was used to evaluate pharmacokinetic parameters and Table 3 shows the obtained results. Fig. 5C represents the HPLC system generated

retention time for FSM and p-nitrophenol at 8.275 and 10.059 min. respectively. The half-life of the chitosan modified PLGA nanoparticles was found to be more than the PLGA nanoparticle and FSM (pure). The maximum concentration of the FSM in FSM-chitosan-conjugated PLGA nanoparticles was found to be after 6 h of the dose administration which is higher than the FSM in which maximum concentration was achieved after 2 h of dose administration. It can be seen that the mean residence time (MRT) for FSM-chitosan-conjugated PLGA nanoparticles was 8.8319 ± 0.93 h which was 6.45 times higher than the FSM. Furthermore, total AUC for FSM-PLGA nanoparticles, FSM-chitosan-coated-PLGA nanoparticles and FSM-chitosan-conjugated PLGA nanoparticles was found to be 2.6, 3.1 and 4.3 times higher than that for FSM at the same dose of 6.6 mg/kg of FSM. The above results indicate that FSM loaded chitosan conjugated PLGA nanoparticles have shown better pharmacokinetic parameters than the FSM loaded PLGA nanoparticles ensuring better sustained effect of the FSM.

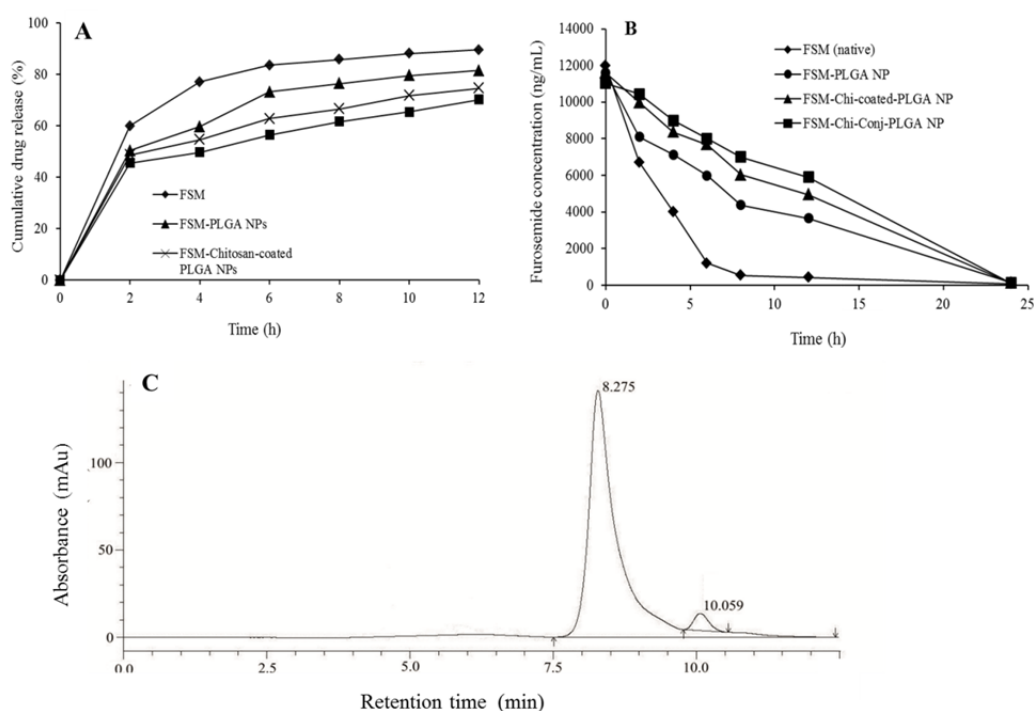


Fig. 5. (A) *In vitro* drug release profile, (B) *in vivo* pharmacokinetic study of FSM; FSM-PLGA-NP, FSM-chi-coated-PLGA-NP, and FSM-chi-conj. PLGA-NP after i.v. injection at an equivalent FSM dose of 6.6 mg/kg. (C) Typical chromatogram, plotted as absorbance (276 nm) vs. elution time, showing the separation and detection of FSM and the internal standard; retention times (min) are 8.275 for FSM and 10.059 for p-nitrophenol. FSM, furosemide; PLGA, Poly (lactide-co-glycolide); FSM-PLGA-NP, FSM loaded PLGA nanoparticle; FSM-chi-coated-PLGA-NP, FSM loaded chitosan-coated PLGA; (FSM-chi-conj. PLGA-NP, FSM loaded chitosan-conjugated PLGA nanoparticle.

Table 3. Pharmacokinetic parameters of furosemide (FSM, pure), FSM loaded poly (lactide-co-glycolide nanoparticles (FSM-PLGA-NP), FSM loaded chitosan-coated PLGA nanoparticles (FSM-chi-coated-PLGA-NP), and FSM loaded chitosan-conjugated PLGA nanoparticles (FSM-chi-conj-PLGA-NP) after *i.v.* injection at an equivalent FSM dose of 6.6 mg/kg. Values represent the mean \pm SD, n= 3.

Pharmacokinetics Parameters	FSM (pure)	FSM-PLGA NP	FSM-chi-coated-PLGA NP	FSM-chi-conj-PLGA NP
Half-life (h)	0.36 \pm 0.11	1.67 \pm 0.23	3.04 \pm 0.72	3.28 \pm 2.01
AUC (ng h/mL)	132263.7 \pm 239	345796.8 \pm 654	414796.7 \pm 2021	576750.6 \pm 2318
Mean residence time (h)	0.54041 \pm 0.05	2.487321 \pm 0.23	4.29869 \pm 0.62	4.631952 \pm 0.93
Volume of distribution (mL/kg)	996.52 \pm 192.11	3236.39 \pm 223.21	3347.76 \pm 342.12	3865.80 \pm 481.31
Clearance (mL/h.kg)	1894.72 \pm 356.54	1339.56 \pm 301.29	893.21 \pm 112.10	725.21 \pm 109.53
Relative bioavailability	-	2.6	3.1	4.3

DISCUSSION

Formulation and optimization studies of FSM-loaded chitosan-conjugated PLGA nanoparticles were accomplished. Pareto chart (Fig. 2) suggests, X_1 and X_2 has significant effect on Y_1 which manifests an increase in X_1 and X_2 increases mean particle diameter and vice-versa. Though the effect of X_3 on Y_1 is not significant but the best result is obtained for higher value of X_1 - X_3 for all the three cases explained by cube plot and evident in Table 1. The effect of the drug and polymer concentration on the nanoparticle size may be due to the higher resultant organic phase viscosity, which leads to larger nanodroplet formation (31). Particle mean diameter was not significantly affected by chitosan ($P > 0.05$) (Fig. 1C), could be due to its low molecular weight. Results of this study have shown that the nanoparticle size is influenced by amount of the drug and polymer and not the type of surfactant used in the preparation of nanoparticles.

The zeta potential of the control PLGA nanoparticles was negative and on coating and conjugating the PLGA nanoparticles with chitosan, the zeta potential was less negative which could be due to the positive charge on the terminal amine group in chitosan (19). The zeta potential of the PLGA nanoparticles was found to be -20.0 ± 2.36 mV (Table 2) which are close to -25 mV of ideal stabilization (32). It has been reported elsewhere that the negative charge on PLGA nanoparticles is due to the ionization of carboxylic end group of surface polymer. Our results presented here are in accordance with the results reported for this system (33). Chitosan conjugation to PLGA was established by FTIR study which

clearly confirms the presence of amide bonds in chitosan-conjugated nanoparticles while it was absent in chitosan-coated nanoparticles which agrees well with the study performed by Chakravarthi *et al.* (34).

Spherical shape of FSM-loaded chitosan-conjugated PLGA nanoparticles with insignificant aggregation was confirmed by SEM study (Fig. 3C₁). TEM study confirmed the absence of significant cracks on the nanoparticle surface (Fig. 3C₂). The nanoparticle size as observed by SEM and TEM correlated well with the size measured by PCS, Zetasizer. With SEM/TEM, the images measured are only two dimensional. Images from an AFM represent data also in 3D view, so that it is possible to measure the height of the nanoparticles quantitatively. 2D and 3D AFM images in Figs. 3A₃ and 3B₃ respectively, showed smooth nanoparticles surface of all the prepared polymeric nanoparticles without any noticeable pinholes. AFM also revealed that all nanoparticles were spherical in shape. The nanoparticles sizes as observed by AFM correlated well with the size measured by PCS, TEM, and SEM.

In PXRD study, all the characteristic peaks of FSM, chitosan, and PLGA were found to be in accordance with their previously reported crystallography (Fig. 4) that agrees well with the study done by Youm *et al.* (26). On comparing the diffraction patterns of physical mixture of FSM and blank nanoparticles (Fig. 4D) and FSM-loaded nanoparticles (Fig. 4E), no significant crystalline deviation was observed, indicating the presence of FSM in its crystal state.

The plasma half-life of the FSM loaded chitosan-conjugated PLGA nanoparticles was found to be 3.28 ± 2.01 h which is 2.9 times

longer than the FSM that suggest the longer circulation time of FSM loaded chitosan-conjugated PLGA nanoparticle than FSM (pure). Higher AUC value of chitosan modified PLGA nanoparticles than the PLGA nanoparticles could be attributed to the presence of chitosan at the surface of PLGA. Short half-life of FSM was in agreement with its higher clearance (CL) value of $1894.72 \pm 356.54 \text{ mLh}^{-1}\text{kg}^{-1}$. In contrast, higher half-life of FSM-PLGA, FSM-chitosan-coated-PLGA, and FSM loaded chitosan-conjugated PLGA nanoparticle was correlated well with their lower CL values 1339.56 ± 301.29 , 893.21 ± 112.10 , and 725.21 ± 109.53 respectively, that goes well with the study done by DJ Greenblatt (35). The higher MRT values of FSM loaded chitosan-conjugated PLGA nanoparticle confirmed the prolonged systemic circulation potential. This may be due to the synergistic sustained effect of the chitosan-PLGA nanoparticles. Volume of distribution (V_d) of FSM loaded chitosan-conjugated PLGA nanoparticle showed significantly higher value (correlated well with the higher value of half-life) than FSM. The overall observation of higher AUC, half-life, MRT, and V_d , and lower CL of FSM loaded chitosan-conjugated PLGA than FSM (pure) evidently indicate that the present formulation design may prove to be the potential approach for enhancing systemic availability and prolonged systemic circulation of FSM.

CONCLUSION

The FSM-loaded nanoparticles were successfully formulated by modified emulsion solvent evaporation method and optimised using 2^3 factorial design. The formulated nanoparticles were characterized for, particle size (PCS), surface morphology (SEM, TEM, and AFM), polydispersity index, entrapment efficiency, *in vitro* drug release studies, and *in vivo* pharmacokinetic studies. The fabricated nanoparticles obeyed all the parameters specified and were found to be in acceptable limits. A slow and sustained *in vitro* drug release was observed at different time intervals. An improved sustained effect was

also observed possibly due to the influence of chitosan conjugation to PLGA nanoparticles. *In vivo* pharmacokinetic studies confirmed that FSM-loaded chitosan conjugated nanoparticles showed significant increase in AUC and proclaimed their prolonged circulation in the blood when compared to FSM-loaded PLGA nanoparticles and FSM-loaded chitosan coated nanoparticles.

ACKNOWLEDGEMENTS

Author Mrs. Sapna Kashyap acknowledges Ministry of Science and Technology Govt. of India, Department of Science and Technology (DST) for the award of inspire fellowship (Inspire Code: IF140154). The author(s) also thank School of Biochemical Engineering, Indian Institute of Technology, Banaras Hindu University, Varanasi, India for providing high performance liquid chromatography facility which was required for the present research work.

REFERENCES

1. Devarakonda B, Otto DP, Judefeind A, Hill RA, de Villiers MM. Effect of pH on the solubility and release of FSM from polyamidoamine (PAMAM) dendrimer complexes. *Int J Pharm.* 2007;345(1-2):142-153.
2. Goodman LS, Gilman A, Brunton LL. 12th ed. Goodman & Gilman's manual of pharmacology and therapeutics. New York: McGraw-Hill Medical; 2008. pp. 671-702,745-760,770-771.
3. Giebisch G. The use of diuretic agent as a probe to investigate site and mechanism of ion transport process. *Arzneimittelforschung.* 1985;35(1A):336-342.
4. Tripathi KD. 6th ed. Essentials of Medical Pharmacology. New Delhi: Jaypee Brothers Medical; 2008. pp. 562.
5. Darandale SS, Vavia PR. Design of a gastroretentive mucoadhesive dosage form of furosemide for controlled release. *Acta Pharm Sin B.* 2012;2(5):509-517.
6. Parveen S, Sahoo SK. Long circulating chitosan/PEG blended PLGA nanoparticle for tumor drug delivery. *Eur J Pharm.* 2011;670(2-3):372-383.
7. Lu JM, Wang X, Marin-Muller C, Wang H, Lin PH, Yao Q, *et al.* Current advances in research and clinical applications of PLGA-based nanotechnology. *Expert Rev Mol Diagn.* 2009;9(4):325-341.
8. Kumari A, Yadav SK, Yadav SC. Biodegradable polymeric nanoparticles based drug delivery

- systems. *Colloids Surf B Biointerfaces*. 2010;75(1):1-18.
9. Mohamed F, van der Walle CF. Engineering biodegradable polyester particles with specific drug targeting and drug release properties. *J Pharm Sci*. 2008;97(1):71-87.
 10. Makadia HK, Siegel SJ. Poly lactic-co-glycolic acid PLGA as biodegradable controlled drug delivery carrier. *Polymers (Basel)*. 2011;3(3):1377-1397.
 11. Muthu MS. Nanoparticles based on PLGA and its co-polymer: an overview. *Asian J Pharm*. 2009;3(4):266-273.
 12. Mainardes RM, Evangelista RC. PLGA nanoparticles containing praziquantel: effect of formulation variables on size distribution. *Int J Pharm*. 2005;290(1-2):137-144.
 13. Faraji AH, Wipf P. Nanoparticles in cellular drug delivery. *Bioorg Med Chem*. 2009;17(8):2950-2962.
 14. Gadad AP, Vannuruswamy G, Chandra PS, Dandagi PM, Mastiholimath VS. Study of different properties and application of Poly lactic-co-glycolic acid (PLGA) nanotechnology: an overview. *Indian Drugs*. 2012;49(12):5-22.
 15. Pandita D, Kumar S, Lather V. Hybrid poly (lactic-co-glycolic acid) nanoparticles: design and delivery prospectives. *Drug Discov Today*. 2015; 20(1):95-104.
 16. Alqahtani S, Simon L, Astete CE, Alayoubi A, Sylvester PW, Nazzal S, *et al.* Cellular uptake, antioxidant and antiproliferative activity of entrapped α -tocopherol and γ -tocotrienol in poly (lactic-co-glycolic) acid (PLGA) and chitosan covered PLGA nanoparticles (PLGA-Chi). *J Colloids Interface Sci*. 2015;445:243-251.
 17. Lim EK, Sajomsang W, Choi Y, Jang E, Lee H, Kang B, *et al.* Chitosan-based intelligent theragnosis nanocomposites enable pH-sensitive drug release with MRI-guided imaging for cancer therapy. *Nanoscale Res Lett*. 2013;8(1): 467-478.
 18. Liu B, Wang H, Fan L, Qiu X, Luo Y, Zhou S, *et al.* Chitosan-modified D- α tocopheryl poly(ethylene glycol) 1000 succinate-b-poly(ϵ -caprolactone-glycolide) nanoparticles for the oral chemotherapy of bladder cancer. *J Appl Polym Sci*. 2013;130(3):2118-2126.
 19. Chung YI, Kim JC, Kim YH, Tae G, Lee SY, Kim K, *et al.* The effect of surface functionalization of PLGA nanoparticles by heparin- or chitosan-conjugated pluronic on tumor targeting. *J Control Release*. 2010;143(3):374-382.
 20. Chen LJ, Burka LT. Chemical and enzymatic oxidation of furosemide: formation of pyridinium salts. *Chem Res Toxicol*. 2007;20(12):1741-1744.
 21. Chronopoulou L, Cutonilli A, Cametti C, Dentini M, Palocci C. PLGA-based nanoparticles: effect of chitosan in the aggregate stabilization. A dielectric relaxation spectroscopy study. *Colloids Surf B Biointerfaces*. 2012;97:117-123.
 22. Ding SJ. Biodegradation behaviour of chitosan/calcium phosphate composites. *J Non-Cryst Solids*. 2007;353(24-25):2367-2373.
 23. Ravi Kumar MN, Bakowsky U, Lehr CM. Preparation and characterization of cationic PLGA nanospheres as DNA carriers. *Biomaterials*. 2004;25(10):1771-1777.
 24. Chakravarthi SS, De S, Miller DW, Robinson DH. Comparison of anti-tumor efficacy of paclitaxel delivered in nano-and microparticles. *Int J Pharm*. 2010;383(1-2):37-44.
 25. Muthu MS, Kuttu RV, Luo Z, Xie J, Feng SS. Theranostic vitamin E TPGS micelles of transferrin conjugation for targeted co-delivery of docetaxel and ultra-bright gold nanoclusters. *Biomaterials*. 2015;39:234-248.
 26. Youm I, Murowchick JB, Youan BB. Entrapment and release kinetics of furosemide from pegylated nanocarriers. *Colloids Surf B Biointerfaces*. 2012;94:133-142.
 27. Muthu MS, Rawat MK, Mishra A, Singh S. PLGA nanoparticle formulations of risperidone: preparation and neuropharmacological evaluation. *Nanomedicine*. 2009;5(3):323-333.
 28. Abou-Auda HS, Al-Yamani MJ, Morad AM, Bawazir SA, Khan SZ, Al-Khamis KI. High-performance liquid chromatographic determination of furosemide in plasma and urine and its use in bioavailability studies. *J Chromatogr B Biomed Sci Appl*. 1998;710(1-2):121-128.
 29. Mills CD, Whitworth C, Rybak LP, Henley CM. Quantification of furosemide from serum and tissues using high-performance liquid chromatography. *J Chromatogr B Biomed Sci Appl*. 1997;701(1):65-70.
 30. Shin S, Oh J, Lee Y, Choi K, Choi J. Enhanced dissolution of furosemide by coprecipitating or cogrinding with crospovidone. *Int J Pharm*. 1998;175(1):17-24.
 31. Govender T, Riley T, Ehtezazi T, Garnett MC, Stolnik S, Illum L, *et al.* Defining the drug incorporation properties of PLA-PEG nanoparticles. *Int J Pharm*. 2000;199(1):95-110.
 32. Muller RH. Charge determination. Muller RH CRC press: Boca Raton; 1991. pp. 57-97.
 33. Betancourt T, Brown B, Brannon-peppas L. Doxorubicin-loaded PLGA nanoparticles by nanoprecipitation: preparation, characterization and *in vitro* evaluation. *Nanomed*. 2007;2(2):219-232.
 34. Chakravarthi SS, Robinson DH. Enhanced cellular association of paclitaxel delivered in chitosan-PLGA particles. *Int J Pharm*. 2011;409(1-2):111-120.
 35. Greenblatt DJ. Elimination half-life of drugs: value and limitations. *Annu Rev Med*. 1985;36:421-427.